Journal of Power Sources 215 (2012) 109–115

Contents lists available at SciVerse ScienceDirect

Journal of Power Sources

journal homepage: www.elsevier.com/locate/jpowsour

Lithium diffusion in sputter-deposited $Li_4Ti_5O_{12}$ thin films

F. Wunde*, F. Berkemeier, G. Schmitz

Institute of Material Physics, University of Münster, Wilhelm-Klemm Str. 10, D-48149 Münster, Germany

HIGHLIGHTS

- Thin Films of $Li_4Ti_5O_{12}$ are deposited by ion beam sputtering.
- XRD and TEM are used to proof the desired structure of the thin films.
- Galvanostatic cycling shows capacity loss at high charging currents.
- A new method is shown to determine the diffusion coefficient of lithium.
- Usage of GITT studies confirms the measured diffusivity.

ARTICLE INFO

Article history:
Received 23 February 2012
Received in revised form
25 April 2012
Accepted 27 April 2012
Available online 8 May 2012

Keywords:
Ion beam sputtering
Lithium ion batteries
Lithium titanium oxide
Chemical diffusion coefficient
GITT

ABSTRACT

$Li_4Ti_5O_{12}$ (LTO) thin films are deposited by dc-ion beam sputtering at different oxygen partial pressures and different substrate temperatures. In order to investigate, how these two parameters influence the atomic structure, the specimens are characterized by X-ray diffraction and transmission electron microscopy. Electrochemical characterization of the films is done by cyclic voltammetry and chronopotentiometry. To determine an averaged chemical diffusion coefficient of lithium, a method is developed, evaluating c-rate tests. The results obtained by this method are compared to results obtained by the well established galvanostatic intermittent titration technique (GITT), which is used to determine a concentration dependent diffusion coefficient of lithium in LTO.

1. Introduction

Generally, the power and power density of a lithium ion battery depends on the electrochemical performance of its individual components, i.e. cathode, anode, and electrolyte. In case of the anode, graphite has been the dominating material in the past and still most of the commercial cells consist of graphite-based anodes, since it offers a reasonable storage capacity for lithium, an acceptable cycling stability, and a low price [1]. Nevertheless, during the last years, other potential anode materials have been found, like tin [2], silicon [3], or lithium titanium oxide (LTO) [4].

From a structural point of view, lithium titanate shows a spinel-type structure, which offers vacancies for lithium storage [5]. So the uptake and release of lithium is described by the following equation [6]

$$Li_4Ti_5O_{12} + 3Li \leftrightharpoons Li_7Ti_5O_{12}. \quad (1)$$

In the case of de-lithiated form of LTO, the permanently bound lithium occupies the tetrahedral sites of the structure, whereas half of the vacant octahedral sites of the spinel framework provide the possibility to intercalate additional lithium ions (Fig. 1). During the uptake of additional lithium within an electrochemical reaction, the permanently bound lithium moves to the octahedral sites [4]. Based on these fundamental assumptions and the size of a unit cell, the theoretical capacity of LTO denotes 60.8 μAh (cm^{-2} μm^{-1}) [4].

The goal of this work is to prepare spinel-structured lithium titanate by ion beam sputtering. The thin film geometry allows using simple models to describe the diffusion process and to study interface effects. Today there are some works in the literature, reporting on thin film preparation by physical deposition methods e.g. pulsed laser deposition [7], magnetron sputtering [6], and rf-sputtering [8]. Nevertheless, these works do not focus on the lithium diffusion in LTO but structural properties, and to our knowledge studies on the lithium diffusivity in LTO have only been performed on thin films deposited, chemically like the sol–gel method [9].

* Corresponding author. Tel.: +49 251 83 36753; fax: +49 251 83 38346.
E-mail address: f_wund01@uni-muenster.de (F. Wunde).

0378-7753/$ – see front matter © 2012 Elsevier B.V. All rights reserved.
doi:10.1016/j.jpowsour.2012.04.102

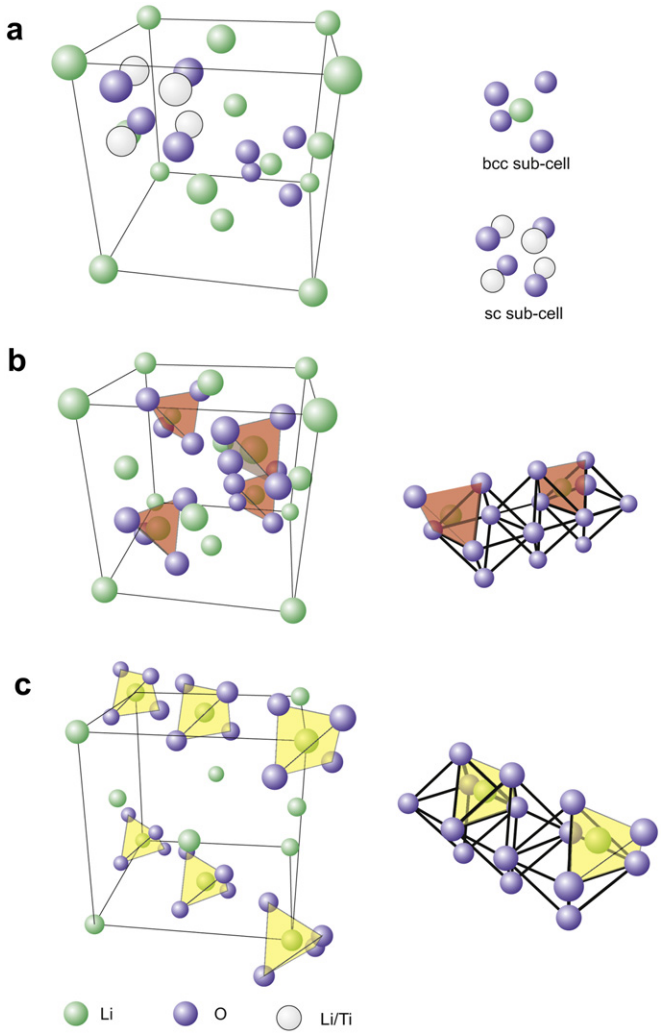

Fig. 1. (a) Spinel lattice structure, exhibiting a fcc main structure, alternating filled with four simple cubic (sc) sub-cells and four body-centered cubic (bcc) sub-cells, respectively. (b, c) Lithium atoms occupy the tetrahedral sites of the spinel, that are all in the proximity of an octahedral site. The octahedral sites are located on a straight line, which is oriented in [110] or [$\bar{1}$10] direction. The sequence of these octahedral sites can be regarded as some kind of diffusion channels.

In this work, X-ray diffraction (XRD) and transmission electron microscopy (TEM) are used after thin film deposition to characterize crystal structure and morphology of thin films in dependence on reactive gas partial pressure and substrate temperature. Cyclic voltammetry (CV) is obtained to characterize the films electrochemically. Finally, the diffusion coefficient of lithium in LTO is determined by galvanostatic cycling and galvanostatic intermittent titration technique (GITT).

2. Experimental

2.1. Thin film deposition

Thin films of LTO were prepared by dc-ion beam sputtering: An ion gun (Roth & Rau) is mounted inside a vacuum chamber of 10^{-8} mbar base pressure, emitting an ion beam of 1 kV argon ions, with a diameter of 4 cm and an intensity of 1.6 mA cm^{-2}. The beam is focused on a target (8 cm diameter), so that target atoms are sputtered of and deposited onto an opposed substrate. The working pressure during sputtering is increased up to 5×10^{-4} mbar. Before hitting the target, the beam is neutralized by a plasma bridge neutralizer. During sputtering, an oscillating quartz sensor measures the deposited film thickness. In order to optimize synthesis conditions, oxygen can be injected as reactive gas up to a partial pressure of 3×10^{-4} mbar and the substrate temperature can be controlled between room temperature and 600 °C [10].

The sputter target was prepared by cold pressing commercial LTO powder (EXM 1037-$Li_4Ti_5O_{12}$, Südchemie). Semiconductor silicon wafers, about 2 cm^2 in size served as substrates. In case of samples used for structural investigations by XRD or TEM, the LTO layers were directly deposited upon the silicon surface. In case of samples used for electrochemical investigations, substrates were thermally oxidized, to form a 200 nm thick SiO_2 layer, that provides electrical isolation. To contact the LTO layer electrically, a metallic current collector is deposited between the substrate and the LTO, consisting of a 25 nm titanium and a 50 nm gold layer. Gold provides the electrical contact to the LTO, whereas titanium enhances the mechanical adhesion to the substrate [6].

2.2. Structural investigations

Sputter-deposited thin films were investigated by XRD using Cu-K_α radiation (Kristalloflex D5000, Siemens) and $\theta/2\theta$ Bragg–Brentano geometry. For deeper structural analysis, electron transparent cross-section samples were prepared by conventional grinding, dimpling, and ion milling [11] and were subsequently investigated using a 200 kV transmission electron microscope (H-800, Hitachi). Via TEM, bright field images, as well as selected area diffraction (SAD), were obtained on the samples.

2.3. Electrochemical investigation

The thin film samples were characterized, electrochemically, to verify their functionality as electrode material. For this purpose, 100 nm thin LTO films, sputter-deposited onto oxidized silicon substrates, covered by a titanium/gold current collector, were measured via cyclic voltammetry, constant current c-rate tests and galvanostatic intermittent titration technique (GITT). All measurements were carried out by a three electrode configuration consisting of the thin film sample (working electrode) and two metallic lithium wires (reference and counter electrode), dipped into a liquid electrolyte (DMC/EC, 1:1 with 1 mol l^{-1} $LiClO_4$) [7,12]. To prevent any contamination by oxygen or water, all measurements were performed inside an argon-filled glove box.

3. Results and discussion

3.1. Structural investigations

In order to optimize the preparation conditions of the LTO layers, films of 250 nm in thickness were prepared at different substrate temperatures and different oxygen partial pressures, respectively. Afterwards, the lattice structure of the samples was investigated by XRD, i.e. the intensity of the most pronounced LTO (111) reflection was evaluated. The results of these measurements, shown in Fig. 2 and Fig. 3, clearly indicate that thin films prepared at a substrate temperature of 600 °C and an oxygen partial pressure of 3×10^{-4} mbar, show most characteristic LTO features.

Additionally, a complete XRD spectrum of a layer, prepared under these favorite conditions is presented in Fig. 4. LTO reflections at 18.4°, 37.5°, 57.2°, and 79.2°, corresponding to (111) lattice planes and higher ordered parallel planes, indicate that deposited films are highly oriented in (111) direction. In addition to these LTO reflections, a pronounced peak of the silicon substrate and a slight signal of a rutile impurity at 39.3° is observed. But since the

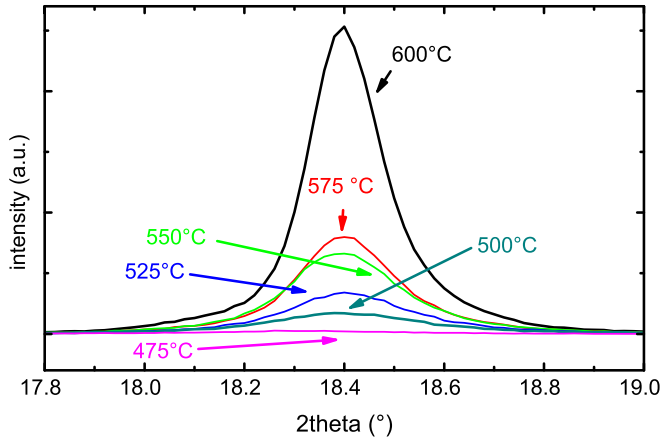

Fig. 2. (111) XRD reflection of 248 nm thin LTO films deposited at 3×10^{-4} mbar O_2 and different substrate temperatures.

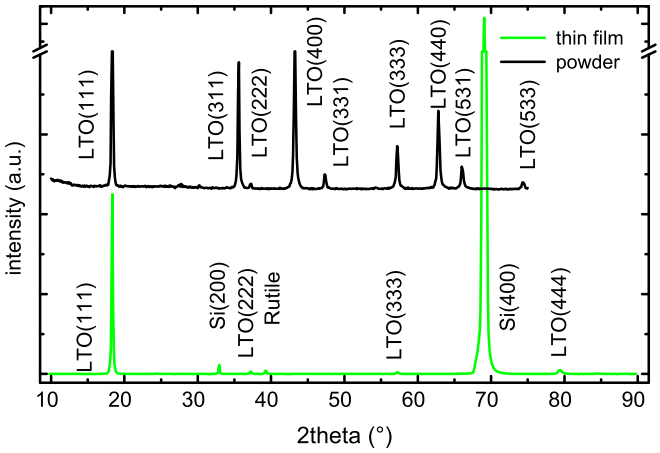

Fig. 4. XRD data of 248 nm thin LTO films, deposited on a silicon substrate at 600 °C and 3×10^{-4} mbar O_2 in comparison with the XRD data of LTO powder material.

intensity of this signal is minor compared to the LTO reflections, we state that this impurity will presumably not affect the electrochemical properties of the LTO layers.

A TEM micrograph of a LTO film cross-section, prepared under optimum conditions, is shown in Fig. 5 (top). The film, exhibiting a thickness of about 500 nm, is dense and smooth with respect to the film thickness. In the corresponding electron diffraction pattern, shown in Fig. 5 (bottom), a crystalline structure is observed, indicated by discrete reflections, which are located on well defined rings, each of them well related to a lattice distance of lithium titanate.

The surface morphology of the thin films was measured using a profiling system (Dektak XT, Bruker) equipped with a tip of 2.5 μm curvature radius. The measurement shows a smooth surface without any pores or pinholes, and proofs the homogeneity of the layer thickness, i.e. a variation of ±10 nm (≈4%) was found within a lateral distance of 1.5 nm (inlet of Fig. 5).

To obtain chemical information about the thin film electrodes, we performed Electron Energy Loss Spectroscopy (EELS) on a LTO layer prepared at optimum conditions (Fig. 6). Since a quantitative analysis of the lithium content is not possible by EELS, due to overlap of the lithium adsorption edge at 55 eV with the plasmon region, we analyzed the chemical shift of the titanium edge. This chemical shift is quite sensitive to the oxidation state, as shown in case of vanadium or cobalt [13]. A comparison between the EELS spectrum of a LTO layer and a TiO_2 reference sample (oxidation state +IV) [14] shows that the chemical shifts of both titanium adsorption edges agrees to each other, within an energy loss of ≈1 eV, indicating an oxidation state of titanium in LTO of +IV, as expected by the stoichiometry of $Li_4Ti_5O_{12}$. This agreement of the oxidation states, and the result of the electron diffraction (Fig. 5) lead us to the conclusion, that the sputter-deposited LTO layers exhibit both, the desired structure and the desired stoichiometry.

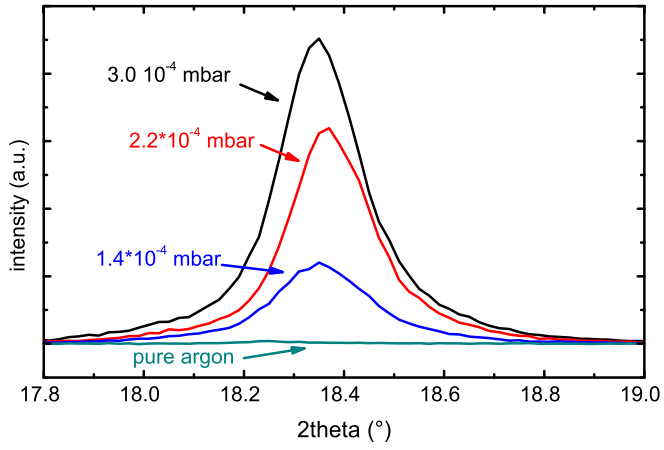

Fig. 3. (111) XRD reflections of 100 nm thin LTO films deposited at 600 °C and different oxygen partial pressures.

3.2. Cyclic voltammetry

Cyclic voltammetry was performed on LTO films between 1 V and 2 V vs. lithium, to investigate their capability of reversible lithium intercalation. The scan rate $\partial_t E = 70\ \mu V\ s^{-1}$ was selected quite small with respect to the film thickness and the estimated diffusivity ($D = 1 \times 10^{-16}\ m^2\ s^{-1}$), to operate the films under quasi-equilibrium conditions.[1] The result of the CV measurement is shown in Fig. 7. Insertion and extraction peaks are sharp and similar in intensity. The insertion current gets its maximum at 1.55 V (FWHM = 0.029 V), while extraction takes place at 1.59 V (FWHM = 0.041 V). Since concentration gradients are neglectable, this difference is explained by a voltage drop at internal ohmic resistances. Double layer capacity and decomposition of the electrolyte cause a current offset, which increases the area under the cyclic voltammogram (see Fig. 7). In order to separate this offset and to determine the charge and discharge capacity, respectively, we use a mathematical expression for quasi-equilibrium cyclic voltammetry given by Aoki et al. [15] and found that the charge capacity can be calculated by using the full width at half maximum Δ, the maximum particle current density j_{max} and the scan rate $\partial_t E$ of the CV curves

$$c_{max} = 1.14 \cdot \frac{\Delta \cdot j_{max}}{d \cdot \partial_t E}. \quad (2)$$

According to Eq. (2), we calculated a capacity of the thin films, which is 24 μAh cm^{-2} μm^{-1} during insertion and 28 μAh cm^{-2} μm^{-1} during extraction of lithium. Additionally, the relationship between the maximum current density and the scan rate was used to estimate a lower limit for the diffusion coefficient. When plotting j_{max} vs. $\partial_t E$, a linear dependence is observed (inlet of Fig. 7) showing that $w = \partial_t E d^2 e / DkT < 1$, and thus for the diffusion coefficient $D > 1 \times 10^{-16}\ m^2\ s^{-1}$ [15,16].

[1] In this case, the parameter $w = \partial_t E d^2 e / DkT$, defined in the work of Aoki et al. [15], is much smaller than one.

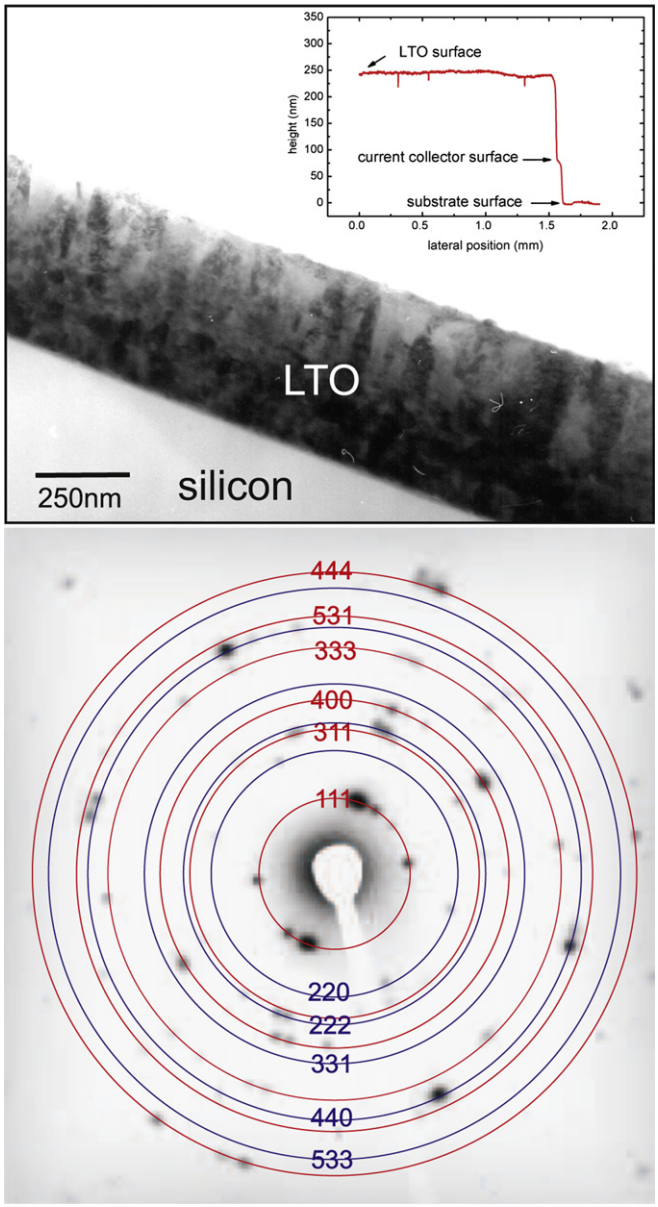

Fig. 5. Cross-section bright field image (top) and SAD image (bottom) of a LTO film, deposited at 600 °C and 3×10^{-4} mbar O_2. Three linear independent lattice planes e.g. (111), (400), (022) of LTO are observed in the diffraction pattern. Inlet shows, a profilometer scan of 150 nm thick LTO film.

3.3. Galvanostatic potentiometry

As reported by Wagemaker et al. [17], tetrahedrally occupied LTO and octahedrally occupied LTO coexist as a solid solution at room temperature and at every state of charge. Therefore, the dependence of the electrical potential of LTO on the lithium content can be described by models of an ideal solution. If volume changes of the LTO lattice during lithium insertion/extraction are neglected, the electrical potential of the LTO depends on the free energy $F(T, V, n)$, which is a function of temperature T, volume V, and number of intercalated lithium atoms n. The free energy itself is characterized by the binding energy of the diffusing species and the configuration entropy. Since the electrical potential E is given by the first derivation of F with respect to n, we get [18]

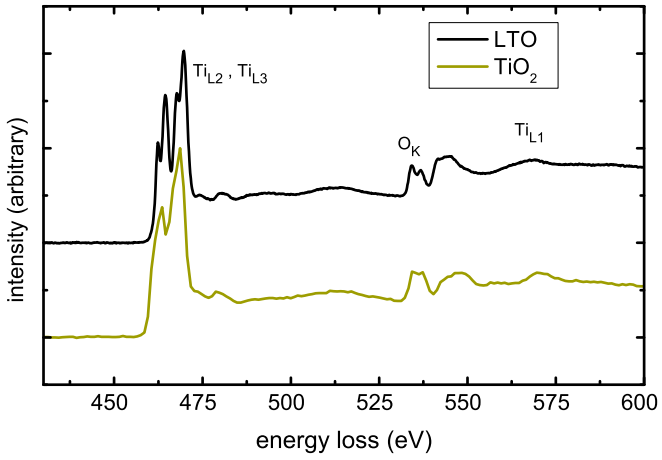

Fig. 6. Electron energy loss spectra of LTO thin film and TiO_2-reference [14].

$$E = \frac{1}{e}\cdot\frac{\partial F}{\partial n}$$
$$\Rightarrow E = E_0 + \frac{kT}{e}\cdot\ln\left(\frac{c_V}{c_{Li}}\right), \quad (3)$$

where the arguments of the logarithm are the concentrations of vacancies and lithium atoms, respectively. It becomes obvious, that according to Eq. (3), the cell voltage exhibits a plateau at moderate lithium contents, and diverges if either the host is completely filled up with lithium or completely depleted. So, the distance between the two divergent arms is proportional to the capacity of the material. Generally, when inserting lithium into LTO by galvanostatic techniques, a concentration gradient of lithium and therefore a gradient of chemical potential is formed inside the layer. In this case, the electrical potential of LTO is determined by the lithium concentration at the surface of the film.

The boundary conditions for this type of measurement are given by

$$\left.\frac{\partial c(x,t)}{\partial x}\right|_{x=0} = -\frac{j_0}{D} \quad (4)$$

$$\left.\frac{\partial c(x,t)}{\partial x}\right|_{x=d} = 0 \quad (5)$$

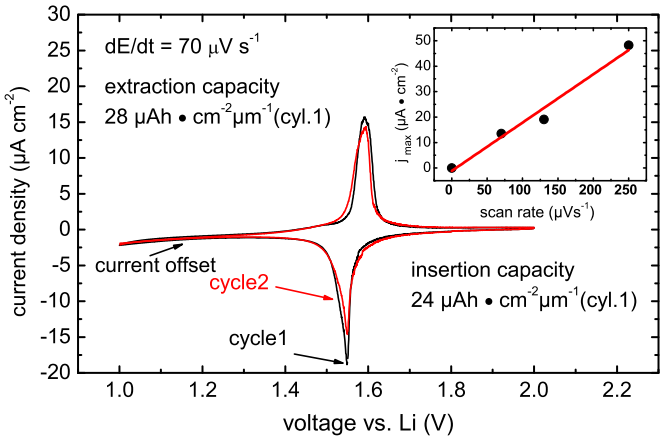

Fig. 7. Cyclic voltammetry on a 100 nm lithium titanate layer.

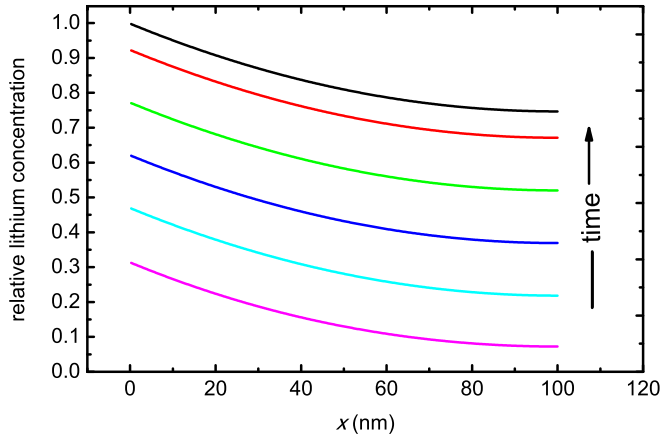

Fig. 8. Concentration profiles of lithium in LTO thin films at different points of time, calculated according to Eq. (8), assuming a current density of 100 μA cm^{-2}.

and

$$c(x, t = 0) = c_0, \tag{6}$$

if the surface of the thin film is set at $x = 0$ and the film thickness is given by d. In Eqs. (4)–(6), j_0 denotes the constant current density and D the chemical diffusion coefficient of lithium in LTO. Since gradients of the chemical potential drive the diffusion, concentration profiles have to solve Fick's second law at any time of the measurement [19]

$$\frac{\partial c(x,t)}{\partial t} = D\frac{\partial^2 c(x,t)}{\partial x^2}. \tag{7}$$

The appropriate solution is calculated elsewhere [20] and is given by

$$c(x,t) = c_0 + \frac{j_0 t}{d} + \frac{j_0 d}{3D} + \frac{j_0}{2dD}x^2 - \frac{j_0}{D}x - \frac{2j_0 d}{D\pi^2}\sum_{n=1}^{\infty}\frac{1}{n^2}\cos\left(\frac{n\pi x}{d}\right)\exp\left(-\frac{Dn^2\pi^2}{d^2}t\right). \tag{8}$$

Resulting concentration profiles within an LTO film, calculated at different points of time and at a fixed current density are shown in Fig. 8.

In thin film approach ($t \gg d^2/D$), the sum in Eq. (8) can be neglected and the concentration of lithium gets parabolic in shape

$$c(x,t) = c_0 + \frac{j_0 t}{d} + \frac{j_0 d}{3D} + \frac{j_0}{2dD}x^2 - \frac{j_0}{D}x. \tag{9}$$

So, the concentration of lithium at the electrolyte side ($x = 0$) is given by

$$c(x = 0, t) = c_0 + \frac{j_0 t}{d} + \frac{j_0 d}{3D}. \tag{10}$$

Eq. (10) shows that in case of intercalation ($j_0 > 0$), the lithium concentration at the surface increases linearly with time, whereas the concentration offset $j_0 d/(3D)$, increases with higher current densities. So, lithium content at the electrolyte side becomes higher with higher current density. Since the electrical potential of the LTO layer is determined by the lithium concentration at the surface of the layer and the charging process is stopped after a certain voltage is reached, the maximum content of lithium that can be intercalated at a given current density is reduced, compared to intercalation at equilibrium conditions

$$c_{\max}^{\exp} = c_{\max}^{\mathrm{eq}} - \frac{j_0 d}{3D}. \tag{11}$$

Thus, the measured charge capacity decreases with increasing charge current density.

In a further measurement, four samples of equal thickness were charged to a potential of 1 V vs. Li, i.e. lithium was inserted into the LTO, using a current density of about 1.4 μA cm^{-2}. The current density was chosen quite low, to make sure that every sample is in the same state of charge. Afterwards, different current densities between 1.4 μA cm^{-2} (≈C/2) to 238.37 μA cm^{-2} (≈95C) were applied to extract lithium. As shown in Fig. 9, the measured capacity decreases with increasing current density and an approximately linear behavior is observed, as presented in Fig. 10. Slight deviation from this behavior may be caused by a concentration dependence of the diffusivity (see Section 3.4).

Due to Eq. (11), the slope m of the fitted line corresponds to the diffusion coefficient, which is found to be

$$D = -\frac{d}{3m} = 3{,}27 \times 10^{-16}\ \mathrm{m^2\ s^{-1}}.$$

3.4. Galvanostatic intermittent titration technique

As shown in Section 3.3, galvanostatic potentiometry can be used to determine a concentration averaged diffusion coefficient, by measuring the available capacity as a function of current density. In previous section, the measured capacity loss has been attributed to a concentration gradient of lithium inside the host, but other effects like degeneration of the host lattice due to high current densities may cause an additional capacity loss.

Therefore, in order to validate the result of Section 3.3, we use GITT to determine the chemical diffusion coefficient of lithium as a function of the lithium concentration [9,20]. This technique applies rectangular-shaped current pulses of constant amplitude and finite duration, while the voltage response of the sample is evaluated. If GITT is performed in thin film approach ($t \gg d^2/D$), the potential $E_0 = E(c_0)$ of the LTO layer before starting the current pulse, increases to

$$E_e = E(c_0 + j_0 t/d + j_0 d/(3D)) \tag{12}$$

at the end of the pulse and finally relaxes to

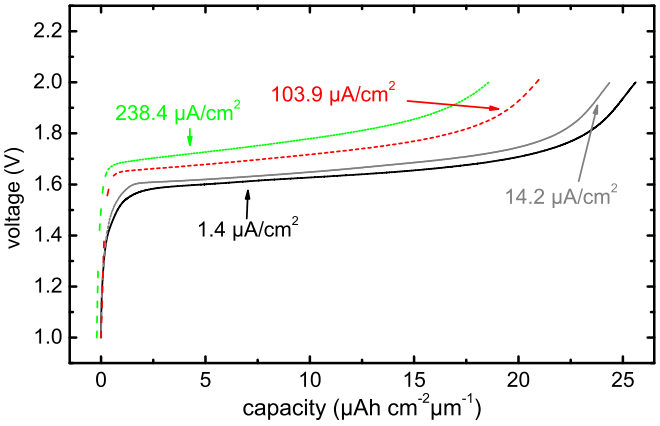

Fig. 9. Galvanostatic chrono-potentiometry obtained at LTO thin films, using different current densities.

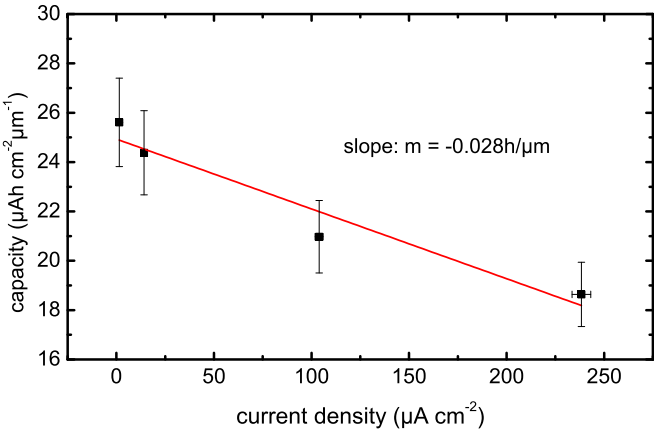

Fig. 10. Capacity of LTO films obtained at different charge current densities. The error bars are due to errors in measurement of the dipped specimen area (2%) and variation of the film thickness (5%).

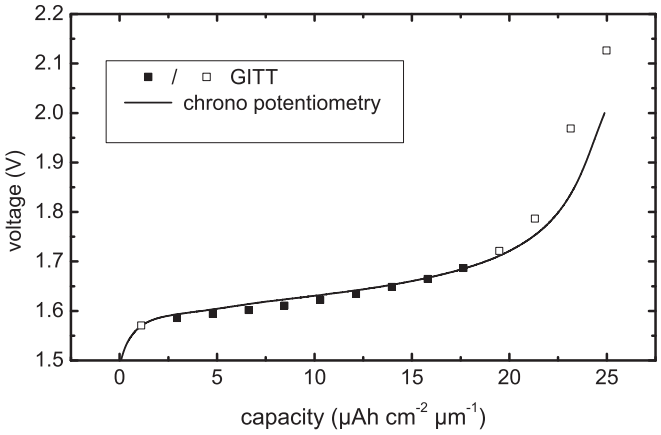

Fig. 12. E_r values obtained during a GITT measurement in comparison to values obtained during a quasi-equilibrium discharge at a constant current of 1.43 µA cm^{-2}. Filled data points are evaluated to determine the lithium diffusivity.

$$E_r = E(c_0 + j_0 t/d) \tag{13}$$

after a sufficient relaxation time (see Fig. 11). Taylor's expansion of Eq. (12) at E_r gives a relationship between these voltages

$$E_e = E_r + \frac{\partial E}{\partial c} \cdot \frac{j_0 d}{3D}$$

$$\Rightarrow D = \frac{j_0 d}{3} \cdot \frac{\frac{\partial E}{\partial c}}{E_e - E_r}. \tag{14}$$

If the GITT measurement is performed in a concentration range, where the potential of the LTO depends quasi-linear on the lithium concentration, $\partial E/\partial c$ can be replaced by the secant line $(E_r - E_0)/\Delta c$. Recalling that Δc is given by $j_0 t/d$, the diffusion coefficient can be calculated [19,21,22]

$$D = \frac{d^2}{3t} \cdot \frac{E_r - E_0}{E_e - E_r}. \tag{15}$$

In this work, GITT measurements were done between 1 V and 2.15 V vs. Li. The relaxed cell voltages E_r are plotted in Fig. 12, in addition to the voltage curve obtained by chrono-potentiometry at a quite low current density of 1.43 µA cm^{-2} (quasi-equilibrium curve of Fig. 9) which is shown for comparison.

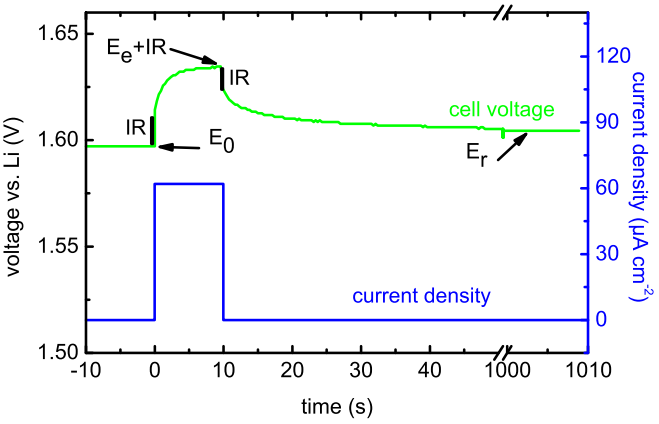

Fig. 11. Example of current and voltage characteristics during a single current pulse of a GITT measurement, obtained on a LTO thin film. *IR* denotes the voltage drop due to ohmic resistance.

Voltage drops due to ohmic resistors and deviations in film thickness cause small deviations between the titration curve and the quasi-equilibrium one. But apart from that, both curves reasonably agree to each other, confirming equilibrium conditions in both types of measurements. Since Eq. (15) is only valid for the linear part of the titration curve, only current pulses that belong to the filled data points of Fig. 12 are used to determine the diffusivity.

The diffusion data obtained from the GITT measurements are shown in Fig. 13 and Table 1, respectively. It is observed that the diffusion coefficient of lithium in the LTO increases with increasing cell voltages, which was also found by Rho et al. in case of sol–gel prepared LTO layers [9]. Since high cell voltages are related to empty hosts, the diffusion coefficient increases, when fewer sites are occupied. In this case lithium atoms do not collide with each other, which results in a more efficient diffusion process in lithium-poor LTO.

Nevertheless, it is reasonable to determine a concentration averaged diffusion coefficient by evaluating c-rate-tests as shown in Section 3.3, since the obtained value of 3.27×10^{-16} m s^{-1} is in quite good agreement with the GITT data, which result in an average diffusivity of 3.95×10^{-16} m^2 s^{-1}. In addition, this

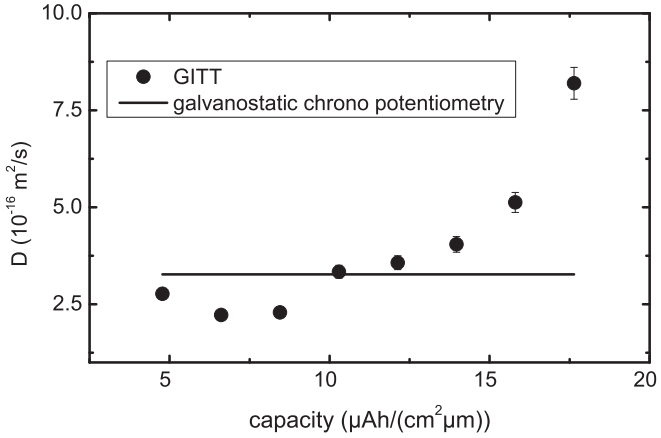

Fig. 13. Diffusion coefficient of lithium in LTO as a function of lithium content, obtained by GITT in comparison to the averaged diffusion coefficient obtained by galvanostatic cycling. In case of the small capacity values, no error bars are shown, since they are negligible compared to the size of the data points.

Table 1
Cell voltages and diffusion coefficients obtained during a GITT measurement.

Pulse	State of charge [μAh cm^{-2} μm^{-1}]	E_r [V]	$E_r - E_0$ [mV]	$E_e - E_r$ [mV]	Diffusivity [m^2 s^{-1}]
2	4.78	1.59	8.16	9.81	2.77E-16
3	6.61	1.60	8.17	12.25	2.22E-16
4	8.45	1.61	8.98	13.07	2.29E-16
5	10.29	1.62	11.4	11.42	3.34E-16
6	12.13	1.63	12.3	11.43	3.57E-16
7	13.96	1.65	13.9	11.44	4.04E-16
8	15.80	1.66	16.3	10.62	5.13E-16
9	17.64	1.69	22.1	9.97	8.20E-16

compliance further indicates that the applied current densities do not damage the LTO in terms of concentration loss.

4. Conclusion

Lithium titanate layers were deposited by ion beam sputtering. Their crystal structure was investigated by XRD and SAD in dependence of synthesis temperature and oxygen partial pressure. A temperature of 600 °C and an oxygen partial pressure of 3×10^{-4} mbar were identified to be the best applicable preparation conditions.

Cyclic voltammetry and galvanostatic chrono-potentiometry show that the films are suitable for reversible storage, providing a capacity of 25 μA cm^{-2} μm^{-1}. The decrease of charge capacity, with increasing charge current densities, was used to measure a concentration averaged diffusion coefficient of lithium, which was found to be 3.27×10^{-16} m^2 s^{-1}. Furthermore, the more complex GITT method was used to measure the concentration dependence of the diffusion coefficient. The comparison of both methods shows that both result in diffusion coefficient that agree quite well to each other, when averaging over the whole on average of the concentration range, and that the observed capacity loss in case of chrono-potentiometry is not caused by a degradation of the active material at high currents, but by concentration gradients within the layers. Since the measured capacity of an electrode material depends on the concentration gradient of Lithium, which is caused by the applied charge/discharge current density, as well as it depends on possible material degradation during the charging/discharging process, the galvanostatic chrono-potentiometry technique may provide the possibility to separate both effects in case of thin film electrodes. In addition to that, it is quite convenient to evaluate c-rate tests on thin film electrodes to measure a concentration-averaged diffusion coefficient, as galvanostatic measurements are standard tests with low complexity.

Acknowledgment

The authors like to thank the German Federal Ministry of Education and Research (BMBF) for financial support.

References

[1] M. Winter, J.O. Besenhard, M.E. Sphar, P. Novak, Adv. Mater. 10 (1998) 725–763.
[2] N. Tamura, R. Ohshita, M. Fujimoto, M. Kamino, S. Fujitani, J. Electrochem. Soc. 150 (2003) A679–A683.
[3] M. Obrovac, L. Christensen, Electrochem. Solid State Lett. 7 (2004) A93–A96.
[4] T. Ohzuku, A. Ueda, N. Yamamoto, J. Electrochem. Soc. 142 (1995) 1431–1435.
[5] J. Bhattacharya, A. van der Ven, Phys. Rev. B 81 (2010) 104304-1–104304-11.
[6] C.-L. Wang, Y. Liao, F. Hsu, N. Tai, M. Wu, J. Electrochem Soc. 152 (2005) A653–A657.
[7] J. Deng, Z. Lu, I. Belharouak, K. Amine, C. Chung, J. Power Sources 193 (2009) 816–821.
[8] P. Birke, S. Döring, S. Scharner, W. Weppner, Ionics 2 (1996) 329–345.
[9] Y. Rho, K. Kanamura, J. Solid State Chem. 177 (2004) 2094–2100.
[10] G. Schmitz, R. Abouzari, F. Berkemeier, T. Gallasch, G. Greiwe, T. Stockhoff, F. Wunde, Z. Phys. Chem. 224 (2010) 1795–1829.
[11] A. Romano, J. Vanhellemont, H. Bender, J. Morante, Ultramicroscopy 31 (1989) 183–192.
[12] Y. Zhao, G. Liu, L. Liu, Z. Jiang, J. Solid State Electrochem. 13 (2009) 705–711.
[13] T. Gallasch, T. Stockhoff, D. Baither, G. Schmitz, J. Power Sources 196 (2011) 428–435.
[14] C.C. Ahn, O.L. Krivanek, EELS ATLAS (1983).
[15] K. Aoki, K. Tokuda, H. Matsuda, J. Electroanal. Chem. 146 (1983) 417–424.
[16] K.A. Striebel, C.Z. Deng, S.J. Wen, E.J. Cairns, J. Electrochem. Soc. 143 (1996) 1821–1827.
[17] M. Wagemaker, D. Simon, E. Kelder, J. Schoonman, C. Ringpfeil, U. Haake, D. Lützenkirchen-Hecht, R. Frahm, F. Mulder, Adv. Mater. 18 (2006) 3169–3173.
[18] M. Landstorfer, S. Funken, T. Jacob, Phys. Chem. Phys. 13 (2011) 12817–12825.
[19] W. Weppner, R. Huggins, J. Electrochem. Soc. 124 (1977) 1569–1578.
[20] H.S. Carslaw, J.C. Jaeger, Oxford University Press (1959) 112.
[21] C. Wen, B. Boukamp, R. Huggins, W. Weppner, J. Electrochem. Soc. 126 (1979) 2258–2266.
[22] P. Birke, W. Chu, W. Weppner, Solid State Ionics 93 (1996) 1–15.